Journal of
Applied Crystallography
ISSN 0021-8898
Editor: **Anke R. Kaysser-Pyzalla**

High-pressure phase transitions and equations of state in NiSi. I. *Ab initio* simulations

Lidunka Vočadlo, Ian G. Wood and David P. Dobson

J. Appl. Cryst. (2012). **45**, 186–196

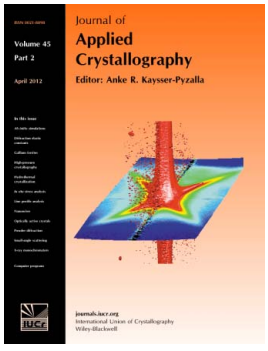

Journal of
Applied Crystallography
ISSN 0021-8898

Received 17 August 2011
Accepted 4 January 2012

High-pressure phase transitions and equations of state in NiSi. I. *Ab initio* simulations

Lidunka Vočadlo, Ian G. Wood* and David P. Dobson

Department of Earth Sciences, University College London, Gower Street, London WC1E 6BT, UK. Correspondence e-mail: ian.wood@ucl.ac.uk

First-principles calculations have been used to determine the equation of state and structural properties of NiSi up to pressures equivalent to that in the Earth's inner core. At atmospheric pressure, the thermodynamically stable phase is that with the MnP structure (as found experimentally). At high pressures, NiSi shows phase transformations to a number of high-pressure polymorphs. For pressures greater than ~250 GPa, the thermodynamically stable phase of NiSi is that with the CsCl structure, which persists to the highest pressures simulated (~500 GPa). At the pressures of the Earth's inner core, therefore, NiSi and FeSi will be isostructural and thus are likely to form a solid solution. The density contrast between NiSi and FeSi at inner-core pressures is ~6%, with NiSi being the denser phase. Therefore, if a CsCl-structured (Fe,Ni)Si alloy were present in the inner core, its density (for the commonly assumed nickel content) might be expected to be ~1% greater than that of pure FeSi.

1. Introduction

Nickel monosilicide (NiSi) is a material of considerable industrial importance that exhibits some unusual physical properties. Films of NiSi are used in forming contacts in microelectronics, especially in the connections to the source, drain and gates of the complementary metal-oxide-semiconductor devices (CMOS devices) that are now used very extensively in digital circuitry. For this purpose NiSi has advantages of lower resistivity and lower consumption of silicon than alternatives such as $TiSi_2$ or $CoSi_2$ (see *e.g.* Lavoie *et al.*, 2006). Recent work (Li *et al.*, 2009) has described the formation of NiSi nanolines with smooth sidewalls and widths as low as 15 nm, indicating that this material can satisfy the requirements of reduced size necessary for the so-called '22 nm technology mode' of CMOS devices introduced by the semiconductor manufacturers in 2011, and possibly also the further reductions to 16 and 11 nm modes scheduled for 2013 and 2015. The physical property of NiSi that shows the most striking behaviour is its thermal expansion. The NiSi crystal structure is orthorhombic, with space group *Pnma* (see below), and, at least above room temperature, its expansion is enormously anisotropic, with the *b* axis contracting strongly throughout the temperature range from 293 to 1223 K; the contraction of the *b* axis is, however, more than offset by the expansion of the *a* and *c* axes, so that the volume expansion remains positive. This anisotropy has been observed both in bulk samples (Wilson & Cavin, 1992; Rabadanov & Ataev, 2002*a*; Perrin *et al.*, 2007, 2008) and in thin films (Detavernier *et al.*, 2003). The thermal expansion of NiSi has implications for its use in microelectronics as the expansion mismatch with respect to silicon will generate residual stresses (Murray *et al.*, 2009).

Our interest in NiSi, however, arises neither from its importance in industry nor from a wish to investigate further its unusual thermal expansion, coming instead from the possible role of NiSi in the deep Earth. To a first approximation, the Earth's core is a homogeneous ball of pure iron; the extent to which it differs from this has profound implications for our understanding of the origin of the core, the early thermal and chemical history of the Earth, and the origin of the geomagnetic field. For over 80 years, the Earth's core has been considered to consist of an iron–nickel alloy, more recently with also a few percent of light alloying elements present, such as Si, C, S, O or H. It is generally assumed that these light elements exert the greatest influence in causing the properties of the core to differ from those of pure iron, and much recent computational and experimental work has been devoted towards understanding their effects (see *e.g.* Birch, 1964; Poirier, 1994; McDonough & Sun, 1995; Vočadlo *et al.*, 1999; Vočadlo, Knight *et al.*, 2002; Dobson *et al.*, 2002, 2003; Vočadlo, Brodholt *et al.*, 2002; Wood *et al.*, 2004). However, despite these efforts, no mineralogical model of the core has yet been published whose properties properly match the observed seismological data. One possible reason for this mismatch lies in the neglect of the influence of the major core alloying element, Ni. Investigation of the physical properties of Fe–Ni–*X* ternary systems will be complex and so, initially, we are studying the binary intermetallic Ni*X* phases to determine the extent to which their properties differ from those of the equivalent Fe*X* phases. The present paper describes the results of computer simulations of NiSi at high pressure for comparison with the high-pressure structures and phase diagram of FeSi, a material that we have studied in some detail (Vočadlo *et al.*, 1999; Vočadlo, Knight *et al.*, 2002;

Dobson *et al.*, 2002, 2003). Somewhat surprisingly, no experimental or computational studies of NiSi at high pressure have yet been reported, although both high-pressure experiments and computer simulations have been performed on Ni_2Si (Errandonea *et al.*, 2008).

In a very early study by Borén (1933) it was suggested that NiSi was isostructural with FeSi, adopting the unusual cubic ($P2_13$) sevenfold-coordinated structure shown by the ε-FeSi phase (see §3.7). Later work, however, showed that NiSi actually adopts the MnP structure, crystallizing in the orthorhombic space group *Pnma*, with $Z = 4$ and cell parameters $a \simeq 5.18$, $b \simeq 3.33$, $c \simeq 5.61$ Å (Toman, 1951). Both Ni and Si atoms sit on the 4*c* special positions at $(x, \frac{1}{4}, z)$; for Ni, $x \simeq 0.008$ and $z \simeq 0.188$, and for Si, $x \simeq 0.679$ and $z \simeq 0.917$. The MnP structure is a distorted form of the hexagonal ($P6_3/mmc$) NiAs structure. The relationship between these two structures is discussed by, for example, Rundqvist (1962). In the MnP structure, each Si atom is surrounded by six Ni atoms, forming a coordination polyhedron that is a distorted trigonal prism, and each Ni atom is surrounded by six Si atoms located at the vertices of a distorted octahedron (see §3.2). More recently, detailed descriptions of the structure of NiSi at 295 and 418 K, based on refinements of single-crystal X-ray data including anharmonic atomic displacement parameters, have been presented by Rabadanov & Ataev (2002*a*,*b*).

However, although the structure of bulk samples of NiSi at atmospheric pressure and room temperature is well established, it appears that transient metastable polymorphism is observed during the formation of thin films of NiSi on silicon substrates. As shown experimentally by, for example, d'Heurle *et al.* (1984), De Keyser *et al.* (2008) and Van Bockstael *et al.* (2009), a hexagonal phase forms as a precursor to the orthorhombic NiSi film. It was suggested by d'Heurle *et al.* (1984) that this phase had the NiAs structure, but the more recent work of De Keyser *et al.* (2008) and Van Bockstael *et al.* (2009) indicates that its structure is more closely related to that of θ-Ni_2Si, a material with a composition range from 33 to 40 at.% Si, which exists metastably at room temperature in the $P6_3/mmc$ $InNi_2$ structure (Bhattacharya & Masson, 1976). The $InNi_2$ structure is closely related to that of NiAs. In NiAs, hexagonal close-packed layers of atoms are stacked in an *ABACA* sequence, with Ni forming the *A* layers and As the *B* and *C* layers; in $InNi_2$ this sequence is maintained but additional Ni atoms are introduced, within the *B* and *C* layers, such that the nickel framework itself has an *ACABA* stacking sequence.

Previous first-principles computational studies of NiSi have been made in both the orthorhombic MnP structure (Connétable & Thomas, 2009) and the hexagonal NiAs structure (Connétable & Thomas, 2010). The same authors also simulated ordered nickel silicide phases with a range of compositions, from Ni_3Si to $NiSi_2$ (Connétable & Thomas, 2011). However, in all cases these simulations were made with the aim of furthering the use of the materials for technological applications and they were, therefore, all concerned with determining the properties of the materials, such as the elastic constants, specific heat [determined experimentally for NiSi by Acker *et al.* (1999)], magnetism, electronic density of states *etc*., at atmospheric pressure; thus, the behaviour of NiSi at gigapascal pressures was not reported. The computational study of NiSi in its experimentally observed MnP structure (Connétable & Thomas, 2009) showed that, at atmospheric pressure, it was highly elastically anisotropic, with the linear incompressibility along the *b* axis much larger than that along the other two axes, that it was metallic with a low density of states at the Fermi surface and that there was no evidence of ferromagnetic ordering (the simulations were athermal, effectively at 0 K). Simulations of both bulk and thin films of NiSi have also been performed by Wu *et al.* (2005). These authors state, incorrectly, that bulk NiSi crystallizes with the cubic ε-FeSi structure and, therefore, their simulations of the bulk material were carried out in this structure and (for comparison) also in the CsCl structure. They concluded that the difference in total energy between CsCl- and ε-FeSi-structured phases of NiSi was small, being 0.12 eV atom^{-1}. Finally, first-principles calculations have been used by Teyssier *et al.* (2008) to investigate the $Co_xNi_{(1-x)}Si$ solid solution. At atmospheric pressure, CoSi crystallizes with the ε-FeSi structure, and it was found that a single-phase solid solution with this structure existed for $0 \leq x \leq 0.35$. For $0.74 \leq x \leq 1$, the material was also single phase, but with the MnP structure. For compositions in the range $0.35 \leq x \leq 0.74$, both structures were present.

In this paper we present, therefore, the first investigation of the high-pressure phase diagram of NiSi by *ab initio* computer simulations. It is apparent that this is more complex than that of FeSi, with a wealth of competing high-pressure phases, but that at the pressures of the Earth's core NiSi and FeSi are likely to be isostructural. Following details of the simulation methodology, we present an account of the thermodynamic stability of the various structures simulated, followed by a detailed description of their crystal chemistry and discussion of the geological significance of the results. These simulations were carried out in advance of a parallel experimental study of the high-pressure phases of NiSi by means of a laser-heated diamond-anvil cell and synchrotron X-ray diffraction, the results of which will be reported separately (Lord *et al.*, 2012).

2. Calculation method

The calculations presented here are based on density functional theory (DFT; Hohenberg & Kohn, 1964) within the generalized gradient approximation (GGA; Wang & Perdew, 1991) implemented in the code *VASP* (Kresse & Furthmüller, 1996), with the projected augmented wave method (Blöchl, 1994; Kresse & Joubert, 1999) used to describe the electronic interactions with the atomic nuclei. The structures selected for the starting positions of each set of simulations were as follows: (i) the orthorhombic (*Pnma*) MnP-type structure, as found experimentally for NiSi at ambient conditions, (ii) an orthorhombic 'anti-MnP' (*Pnma*) structure, formed by exchanging the coordinates of all of the Ni and Si atoms, (iii) a structure with space group *Pbma* formed by exchanging the coordinates of two of the four Ni and Si atoms in the unit cell

of the *Pnma* structure in its high-pressure form (see §3.4), (iv) a structure formed by *ABAB* stacking of alternating close-packed planes of Ni and Si atoms, equivalent that of WC (Leciejewicz, 1961), (v) the cubic ($P2_13$) ε-FeSi structure as found experimentally for FeSi at ambient conditions, (vi) the CsCl structure, as found in FeSi at high pressures (Vočadlo *et al.*, 1999; Dobson *et al.*, 2002), (vii) the NiAs structure, (viii) the anti-NiAs structure, and (ix) the NaCl structure. Structures (i), (v) and (vi) were chosen as they correspond to known NiSi or FeSi phases; structures (iii) and (iv) were simulated following the discovery that above ∼42 and ∼63 GPa the MnP structure of NiSi spontaneously transformed in the *VASP* simulation into two further structures based on close-packed planes of atoms (as described in §3.3); structures (vii)–(ix) were included for completeness and for comparison with earlier simulations of FeSi (Vočadlo *et al.*, 1999).

The calculations were carried out using the primitive unit cells for the MnP-, 'anti-MnP'-, *Pbma*-, WC-, ε-FeSi-, CsCl-, NiAs- and anti-NiAs-type structures of NiSi and the conventional face-centred cubic unit cell for the NaCl type. They were performed with spin polarization, although no magnetic moments remained on the atoms after energy minimization for any of the structures simulated. An energy cutoff of 700 eV was used for all structures, together with an electronic minimization convergence criterion of 10^{-6} eV in the internal energy. Where appropriate, an atomic minimization convergence criterion of 10^{-4} eV was used. The number of sampling points in reciprocal space used in the calculations was increased until further increase produced a change of less than 0.001 eV atom^{-1} in the calculated internal energy. This convergence condition required the use of, for example, a $7 \times 7 \times 7$ grid of k points for the MnP-type structure (and all other *Pnma* and *Pbma* structures), leading to 64 k points in the symmetry-irreducible volume of the Brillouin zone; sampling points with similar separations in reciprocal space were used for the other structures. For selected materials, calculation of the electronic density of states (DOS) of the materials was also made; this was done at intervals of approximately 0.12 eV in energy. We believe, therefore, that the present calculations are sufficiently accurate for our discussion of the different potential NiSi polymorphs.

The procedure adopted to determine the equations of state was to use *VASP* to calculate the internal energy (E) of the crystal at a set of chosen volumes (V). For the NaCl and CsCl modifications there are no structural parameters to relax; the NiAs-, anti-NiAs- and WC-type structures require relaxation of the c/a ratio. In the case of the cubic ε-FeSi-type structure, the fractional coordinates of both Ni and Si were allowed to vary, whilst in the case of the orthorhombic MnP structure and the other structures with space groups *Pnma* or *Pbma*, both the cell parameters and the fractional coordinates were relaxed. With the exception of the *Pbma* structure (which was generated from a high-pressure form of the *Pnma* structure) all simulations were made along a path of decreasing volume. During the calculations the program parameters were set such that the symmetry of the crystal was maintained and, therefore, phase transitions to structures with lower symmetry were forbidden. The converse, however, is not true and transitions to structures whose space groups are supergroups can occur, as the atoms are not prevented from moving into a more symmetrical arrangement. Since the calculations were athermal and, therefore, equivalent to $T = 0$ K, the pressure (P) at any point on the E *versus* V curve may be found using the standard thermodynamic result $P = -(\partial E/\partial V)_{T=0}$ (see *e.g.* Pippard, 1966), the actual values being determined by fitting the $E(V)$ curve to an integrated Birch–Murnaghan third-order equation of state (EoS; see *e.g.* Vočadlo *et al.*, 1999). Knowing P, V and E, the enthalpy, H, may be calculated. Since $T = 0$, the enthalpy is equal to the Gibbs free energy, G, and thus the most stable phase at any given pressure may be determined. For the special case of ambient pressure ($P \simeq 0$, $T = 0$), $G = E$ and the relative stability of the different polymorphs can be determined simply from the positions of the minima in the E *versus* V curves.

3. Results and discussion

3.1. Thermodynamic stability of the high-pressure phases of NiSi

Fig. 1 shows the internal energy as a function of volume for all of the simulated structures of NiSi in the low-pressure region ($10 < V < 13$ Å^3 atom^{-1}); the stable phase at atmospheric pressure is clearly that with the MnP structure as this has the lowest lying energy minimum. The lines shown in the figure are fits to third-order Birch–Murnaghan equations of state (the EoS parameters are listed in Table 1). However, in the case of the MnP structure, this equation of state was found to give rather poor agreement with the calculated energies when fitted over the full volume range of the calculations ($5 < V < 15$ Å^3 atom^{-1}). Closer examination of the results for this phase revealed that, as the volume was reduced, there were clear discontinuities in the unit-cell parameters (Fig. 2*a*) at

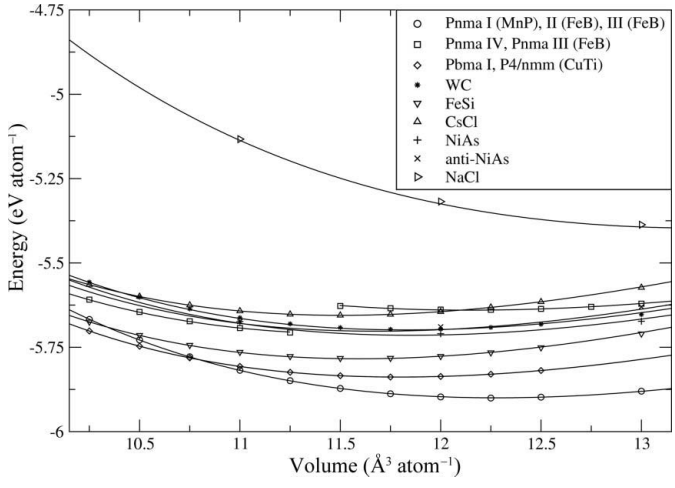

Figure 1
Internal energy *versus* volume of NiSi for all of the different structure types considered, showing the phase transition from the *Pnma*-I (MnP) to the *P4/nmm* (CuTi) structures (indicated by the crossing of the E–V curves at ∼10.75 Å^3 atom^{-1}). For details see text.

Table 1
Equation of state parameters for all NiSi structures simulated, obtained by fitting the internal energy *versus* volume to integrated third-order Birch–Murnaghan equations of state.

Values in brackets are estimated standard uncertainties and refer to the least significant digit. The apparently poorly determined values for some phases arise from the limited volume range over which they exist.

	V_0 (Å^3 atom^{-1})	K_0 (GPa)	K_0'	E_0 (eV atom^{-1})	Volume range fitted (Å^3 atom^{-1})
Pnma-I (MnP)	12.277 (3)	160.572 (2)	4.47 (6)	−5.8998 (2)	10.25–15.0
Pnma-II (FeB)	13.1 (4)	79.3 (2)	5.5 (8)	−5.93 (3)	9.0–10.0
Pnma-III (FeB)†	11.21 (1)	213.402 (8)	4.190 (6)	−5.653 (3)	5.0–8.75
Pnma-IV‡	12.15 (1)	118.188 (8)	4	−5.6400 (4)	11.5–15.0
Pbma-I	11.51 (2)	195.78 (1)	4.172 (7)	−5.784 (4)	5.25–8.75
*P*4/*nmm* (CuTi)	11.7938 (1)	164.7300 (6)	4.85 (1)	−5.83827 (1)	10.25–12.5
WC	11.83 (1)	166.539 (8)	4.31 (1)	−5.699 (1)	5.0–13.0
ε-FeSi	11.593 (3)	180.143 (4)	4.48 (1)	−5.7841 (3)	7.0–12.5
CsCl	11.5020 (5)	173.1770 (6)	4.488 (2)	−5.65525 (4)	7.0–12.5
NiAs	11.85 (3)	163.01 (2)	4.35 (3)	−5.714 (4)	5.0–13.0
Anti-NiAs	11.68 (2)	169.46 (2)	4.38 (3)	−5.702 (4)	5.0–15.0
NaCl	13.30 (3)	151.57 (1)	4.10 (2)	−5.397 (3)	5.0–15.0

† Parameters for the *Pnma*-III (FeB) phase as generated on compression of the *Pnma*-I (MnP) structure. ‡ K_0' was fixed at 4 for this phase, corresponding to a second-order Birch–Murnaghan EoS, as the fit to the third-order EoS was unstable.

∼10.1 and ∼8.8 Å^3 atom^{-1}, indicating that spontaneous transformations to two different structures had occurred during the simulation.[1] Inspection of the atomic coordinates later revealed that there had been no change in space group and that both of these structures (here labelled phases *Pnma*-II and *Pnma*-III) were of the FeB type [see §3.3 for a description of these structures; note that we have found it convenient in this work to label hypothetical high-pressure phases by their space group, followed by an identifier (I, II *etc*.), and then by their structure type, if known]. When these three phases were fitted separately (over volume ranges $10.25 \leq V \leq 15$ Å^3 atom^{-1}, $9 \leq V \leq 10$ Å^3 atom^{-1} and $5 \leq V \leq 8.75$ Å^3 atom^{-1}) much better agreement between the calculated energies and those from the corresponding equations of state was achieved. However, as will be shown below, only the MnP structure and phase *Pnma*-III (FeB) are thermodynamically stable. Compression of a starting structure corresponding to the 'anti-MnP' phase resulted in a similar spontaneous transition to the *Pnma*-III (FeB) structure; the unit-cell parameters from this simulation are also shown in Fig. 2(*a*). Another spontaneous phase transition was observed on increasing the volume of a structure with *Pbma* symmetry (here labelled phase *Pbma*-I), formed by varying the stacking of the close-packed layers found in *Pnma*-III (see §3.4). In this case, the transition, to a tetragonal structure with space group *P*4/*nmm* (a supergroup of *Pbma*) and an atomic arrangement corresponding to that of CuTi (see §3.4), appeared to be continuous, as indicated by the change in cell parameters (Fig. 2*b*).

Fig. 1 clearly shows that at zero pressure the thermodynamically stable phase of NiSi is that with the MnP structure, but that a transition occurs to the *P*4/*nmm* (CuTi) structure at a pressure (∼23 GPa) corresponding to the slope of the common tangent of their *E*–*V* curves. At higher pressures, further transitions occur. These cannot be so readily seen in *E*–*V* plots but can be better observed by using the equations of state to calculate the enthalpy of each phase as a function of pressure (since the calculations were performed at 0 K, the enthalpy is equal to the Gibbs free energy). Fig. 3 shows the difference in enthalpy between each of the relevant phases of NiSi and that of NiSi in the CsCl structure (those phases not shown in Fig. 3 all had enthalpies sufficiently high as to make them always thermodynamically unstable). From Fig. 3 it can be seen that the thermodynamically stable phases of NiSi and the pressure ranges over which they occur are as follows: (i) the MnP structure (as observed experimentally), $0 < P <$ ∼23 GPa; (ii) the *P*4/*nmm* (CuTi) structure, ∼23 < *P* <

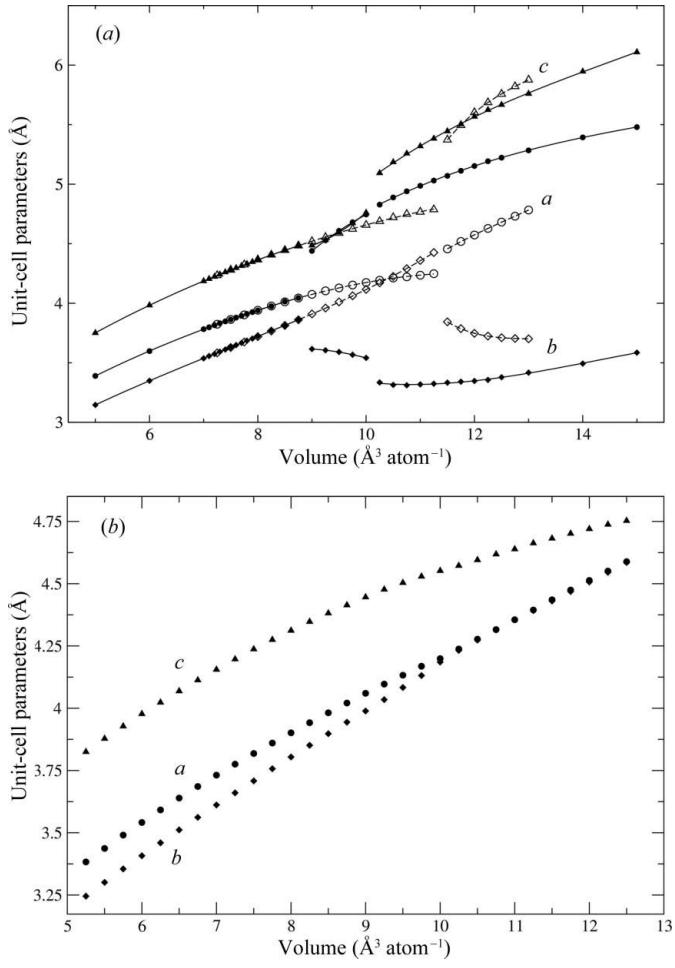

Figure 2
Unit-cell parameters of NiSi as a function of volume. (*a*) Simulations starting from the orthorhombic *Pnma*-I MnP structure (closed symbols) and also from an 'anti-MnP' structure (open symbols) in which the positions of all of the Ni and Si atoms were interchanged. The discontinuous transitions to the isosymmetric higher-pressure phases, *Pnma*-II (FeB) and *Pnma*-III (FeB), are clearly visible. (*b*) Simulations starting with the orthorhombic *Pbma*-I structure described in §3.4, showing the continuous transition to the tetragonal *P*4/*nmm* (CuTi) phase. The lines shown in (*a*) are polynomials fitted to the data points, drawn to provide guides for the eye.

[1] The data used to plot Figs. 2, 5, 9 and 10 are available from the IUCr electronic archives (Reference: KS5298). Services for accessing these data are described at the back of the journal.

Table 2
Simulated ambient-pressure structural parameters for NiSi compared with experimental data; the Ni and Si atoms are both in the 4*c* special positions in space group *Pnma*, with coordinates (x, $\frac{1}{4}$, z).

	Simulated (present work)	Experimental (295 K) (Rabadanov & Ataev, 2002*a*, model 1)
a (Å)	5.1924	5.1752 (7)
b (Å)	3.3640	3.3321 (5)
c (Å)	5.6230	5.6094 (9)
V (Å^3)	98.216	96.73 (1)
Ni: x	0.00745	0.00779 (2)
Ni: z	0.18905	0.18752 (2)
Si: x	0.68057	0.67872 (6)
Si: z	0.91654	0.91750 (6)

~61 GPa; (iii) the *Pbma*-I structure, ~61 < P < ~168 GPa; (iv) the *Pnma*-III (FeB) structure, ~168 < P < ~247 GPa; and (v) the CsCl structure, P > ~247 GPa. Fig. 3 also shows that, although the ε-FeSi phase is never thermodynamically stable, the free energy difference between the ε-FeSi and *Pbma*-I structures is very small, ranging only between 8 and 12 meV atom^{-1}. Phase *Pnma*-II is also never thermodynamically stable, but it may possibly exist metastably, formed by compression of the MnP structure, between ~42 and ~63 GPa. Finally, it should be pointed out that, since the *VASP* simulations were athermal, the results shown in Fig. 3 define the phase diagram at 0 K; whether this sequence of phases remains at higher temperatures will depend on the Clapeyron slopes of the phase boundaries.

3.2. Crystal structure of the ambient-pressure MnP phase of NiSi (*Pnma*-I)

Table 2 shows the calculated cell parameters and fractional coordinates for the ambient-pressure MnP phase of NiSi, together with those determined experimentally by Rabadanov & Ataev (2002*a*), who fitted their experimental data to three models, two of which included anharmonicity in the description of the thermal vibrations. The range in atomic coordinates resulting from these different fits was ~0.0001 for Ni x, ~0.0003 for Ni z, ~0.0002 for Si x and ~0.0008 for Si z; the values shown in Table 2 are those for the simplest approximation, 'Model 1' of Rabadanov & Ataev (2002*a*), in which standard anisotropic harmonic thermal parameters were used. The *VASP* calculations were performed at a volume corresponding to zero pressure (V_0 in Table 1). It can be seen that the agreement with the experimental values is excellent, with the fractional coordinates of the atoms all within 0.001 of the experimental results. The calculated cell volume is slightly larger (by ~1%) as expected from DFT–GGA methodology. Thus we consider that the *VASP* simulations provide an accurate representation of the real material.

The NiAs structure, from which the MnP structure is derived, is composed of close-packed layers of atoms, with the stacking sequence *ABACA*, where the *A* layers are composed of Ni atoms and the *B* and *C* layers are composed of As atoms. The MnP structure is formed by distorting the NiAs structure, producing close-packed layers that are offset from each other and buckled. A projection of the crystal structure of the MnP phase of NiSi down [100] is shown in Fig. 4. As discussed by *e.g.* Rundqvist (1962), this projection corresponds to viewing the NiAs parent structure perpendicular to the close-packed planes of atoms. The hexagonal cell of the corresponding NiAs structure is also shown in the figure, and the atoms are labelled in accordance with the distorted close-packed planes in which they lie. The distortion from the NiAs to the MnP structure results in sixfold primary coordination of both Ni and Si by atoms of the other species. The Ni atoms are coordinated by six Si atoms at the vertices of an octahedron, whereas the six Ni atoms surrounding each Si atom form a trigonal prism; in

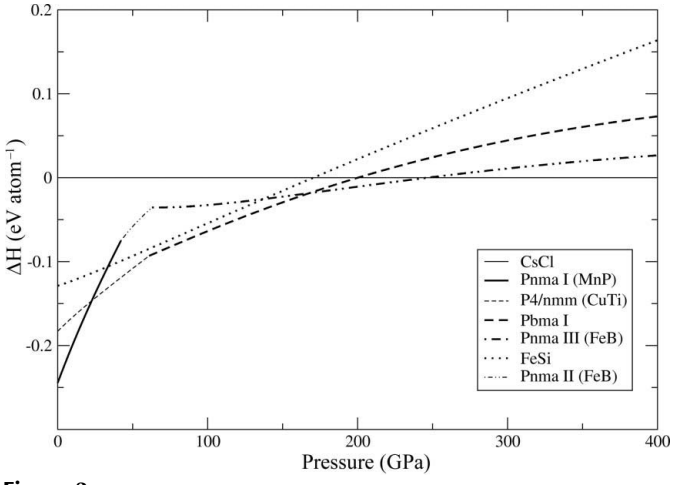

Figure 3
Enthalpy (here equal to the Gibbs free energy) of NiSi phases as a function of pressure, relative to that of the CsCl structure. With increasing pressure the sequence of stable phases is MnP → *P*4/*nmm* (CuTi) → *Pbma*-I → *Pnma*-III (FeB) → CsCl; transition pressures are 23, 61, 168 and 247 GPa, respectively. Note that the free energy difference between the ε-FeSi and *Pbma*-I structures is only 8–12 meV atom^{-1}.

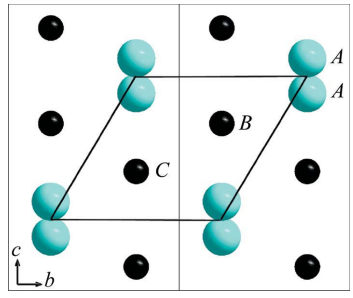

Figure 4
The ambient-pressure MnP-structured phase of NiSi viewed along [100] (phase *Pnma*-I, coordinates taken from Table 2, present work). Two unit cells are shown and the Si atoms are depicted by the smaller darker spheres. This projection corresponds to viewing the NiAs parent structure down [001], perpendicular to the close-packed planes of atoms (*e.g.* Rundqvist, 1962) and the outline of the hexagonal NiAs pseudo-unit cell is also indicated. The close-packed layers in which the atoms would lie in the NiAs parent structure are labelled *A*, *B*, *C* and the stacking sequence in NiAs is *ABACA*. To transform the MnP structure to that of NiAs, the Ni atoms in the *A* layers must be displaced so that they overlie each other in this view, the Si atoms in the *B* and *C* layers must lie above and below the geometric centres of the equilateral triangles formed by the Ni atoms, and, finally, each layer must be flat (which, in the case of the MnP structure, they are not).

both cases the six coordinating atoms lie at distances in the range 2.29–2.41 Å (as determined from the *VASP* simulation). It is of interest to note that, despite the large negative thermal expansion of the *b* axis of NiSi above room temperature (see §1), the behaviour of the cell parameters as a function of volume (and hence of pressure) shown in Fig. 2(*a*) indicates that the axial compressibility of the *b* axis is positive (as it is for the *a* and *c* axes also). The MnP-structured phase of NiSi is not, therefore, expected to show negative linear compressibility, a conclusion which is confirmed by calculation of the axial incompressibilities [$\kappa_i = 1/(s_{i1} + s_{i2} + s_{i3})$, where s_{ij} are the elastic compliances] from the elastic constant values of Connétable & Thomas (2009).

The manner in which the MnP-structured NiSi distorts to form the high-pressure phases *Pnma*-II and *Pnma*-III is described in the following section.

3.3. Crystal structures of the high-pressure phases of NiSi with *Pnma* symmetry, derived from compression of its ambient-pressure structure, *Pnma*-I (MnP): phases *Pnma*-II (FeB) and *Pnma*-III (FeB)

In simulations starting with the orthorhombic (*Pnma*) MnP structure there are clear discontinuities in the cell parameters (Fig. 2*a*) as the volume is reduced, corresponding to high-pressure phase transitions. Similar discontinuities are also found in the atomic fractional coordinates, as shown in Fig. 5. Both of the high-pressure phases have the same orthorhombic symmetry (*Pnma*) as the MnP structure. As a consequence of the simulation method used, lowering of symmetry would not be expected. Although an increase in symmetry is possible, examination of these structures, both visually and by using the 'find symmetry' facility in the program *Endeavour* (Putz *et al.*, 1999; Crystal Impact, 2010), showed that this had not occurred; these phases were, therefore, labelled *Pnma*-II and *Pnma*-III; note that a similar spontaneous phase transformation to the *Pnma*-III structure (origin shifted by *c*/2) also occurred at high pressure in simulations starting with the atoms arranged in an 'anti-MnP' structure (see §3.5).

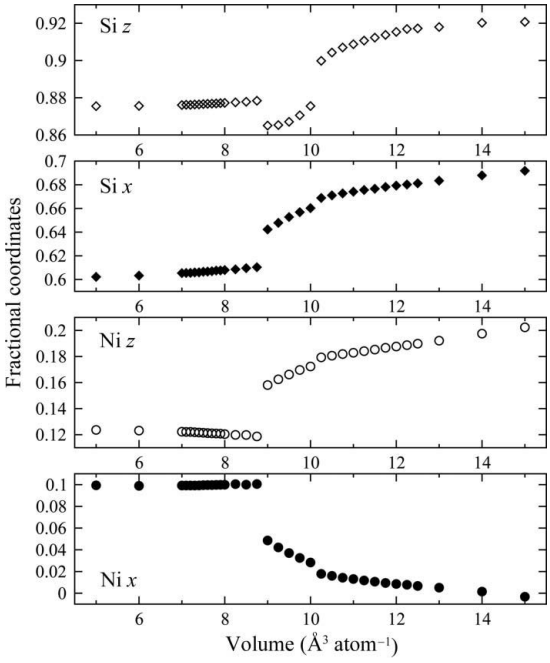

Figure 5
Fractional atomic coordinates of NiSi as a function of volume for simulations starting with the orthorhombic *Pnma*-I (MnP) structure; the transitions to the isosymmetric higher-pressure phases *Pnma*-II (FeB) and *Pnma*-III (FeB) are clearly visible [the corresponding cell parameters are shown in Fig. 2(*a*)].

Examination of the atomic coordinates revealed that both of these crystal structures are based on *ABAB* stacking of hexagonal close-packed layers. The layers, however, now lie perpendicular to the *b* axis of the orthorhombic unit cell (*i.e.* perpendicular to the distorted close-packed layers of the MnP-structured phase) and contain both Ni and Si atoms. The manner in which the layers develop is shown in Fig. 6. Figs. 6(*a*), 6(*b*) and 6(*c*) show, respectively, the layers of Ni and Si atoms at $y = \frac{1}{4}$ at simulation volumes of 12.277 Å^3 atom^{-1} [0 GPa – phase *Pnma*-I (MnP)], 9 Å^3 atom^{-1} [∼84 GPa – phase *Pnma*-II (FeB)] and 5 Å^3 atom^{-1} [∼965 GPa – phase *Pnma*-III (FeB)]. It can be seen that, as the pressure increases, the atoms (primarily the Si atoms) are displaced such that they

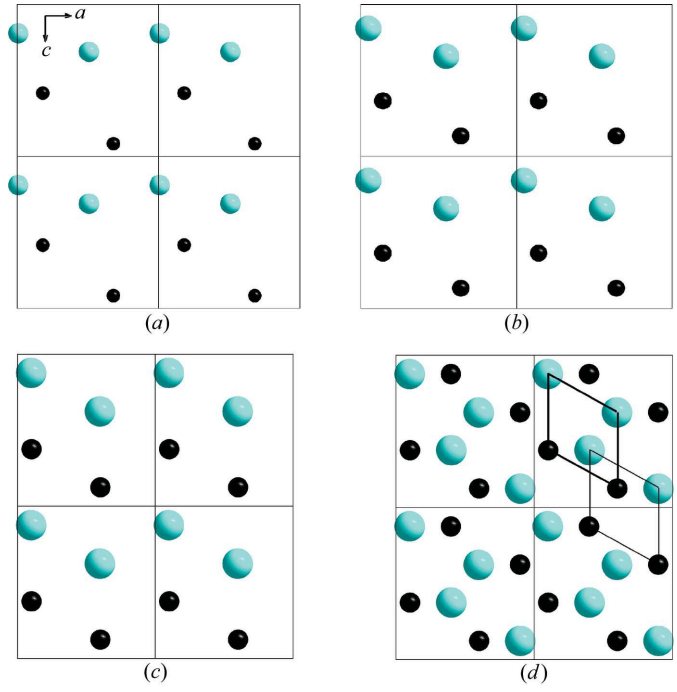

Figure 6
Development of the high-pressure phases *Pnma*-II (FeB) and *Pnma*-III (FeB) from the *Pnma*-I (MnP) structure. All diagrams show the planes of atoms at $y = \frac{1}{4}$, viewed along [010]; the Si atoms are depicted by the smaller darker spheres. So that the evolution of the fractional coordinates can be more readily compared, the scales of the diagrams have been adjusted (such that the length of the *c* axis remains the same) to remove the reduction in unit-cell size as the pressure increases. Four unit cells are shown, and the directions of the *a* and *c* axes are as given in (*a*) throughout. (*a*) *Pnma*-I (MnP) structure at 12.277 Å^3 atom^{-1} (0 GPa); (*b*) *Pnma*-II (FeB) structure at 9 Å^3 atom^{-1} (∼84 GPa); (*c*) *Pnma*-III (FeB) structure at 5 Å^3 atom^{-1} (∼965 GPa); (*d*) as for (*c*) but also including the plane of atoms at $y = \frac{3}{4}$, so as to show the complete crystal structure formed by *ABAB* stacking of these layers; heavy and light lines outline the pseudo-cells of the layers at $y = \frac{1}{4}$ and $y = \frac{3}{4}$, respectively.

tend to lie on a hexagonal grid, *i.e.* to form a close-packed layer. In phase *Pnma*-II (Fig. 6*b*) the transformation is not complete and the lines of atoms are not straight but form a zigzag; for phase *Pnma*-III, at the highest pressure simulated (Fig. 6*c*), the hexagons of atoms are almost perfect, with the angles deviating from 60° by 2° or less, and the lines of atoms are straight. However, the hexagonal symmetry of the resulting close-packed layer is, of course, broken as the atoms are not all of the same type. The layer produced corresponds to one of the possibilities for close packing of spheres of two kinds discussed by Wells (1986). Fig. 6(*d*) shows how the crystal structures of both phases *Pnma*-II and *Pnma*-III are then constructed by *ABAB* stacking of these layers along the *b* axis.

Inspection of the Inorganic Crystal Structure Database (ICSD; Fletcher *et al.*, 1996) revealed that FeB (see *e.g.* Saltykov *et al.*, 2009; Bjurstroem & Arnfelt, 1929) adopts a similar crystal structure to the *Pnma*-II phase of NiSi, and since phase *Pnma*-III is simply a less distorted variant we have also allocated it to this structure type. The difference between the *Pnma*-II and *Pnma*-III structures of NiSi lies in the primary coordination of the atoms. In *Pnma*-II, the sixfold coordination of each atom in the MnP structure can be considered to have increased to 11-fold; each Ni atom is now surrounded by seven Si and four Ni atoms (at distances between 2.18 and 2.38 Å) and each Si atom is surrounded by seven Ni and four Si atoms (at distances between 2.18 and 2.52 Å). In the *Pnma*-III structure, both atoms have almost perfect 12-fold anticuboctahedral coordination by eight atoms of the other kind and four atoms of the same kind (at distances between 1.87 and 1.96 Å). Calculation of the electronic DOS shown in Fig. 7 revealed that all of the *Pnma* phases (I, II and III) were metallic but that their Fermi energies were such that they corresponded to the positions of minima in their DOS, as observed for the ambient-pressure phase of NiSi by Connétable & Thomas (2009); it can be seen that this feature of the DOS becomes more pronounced as pressure increases. Finally, it should be noted that if phase *Pnma*-II were to exist it would be one of relatively few simple inorganic materials having negative linear compressibility, since Fig. 2(*a*) shows that the *b* axis of this phase lengthens as the volume is reduced, *i.e.* as the pressure is increased.

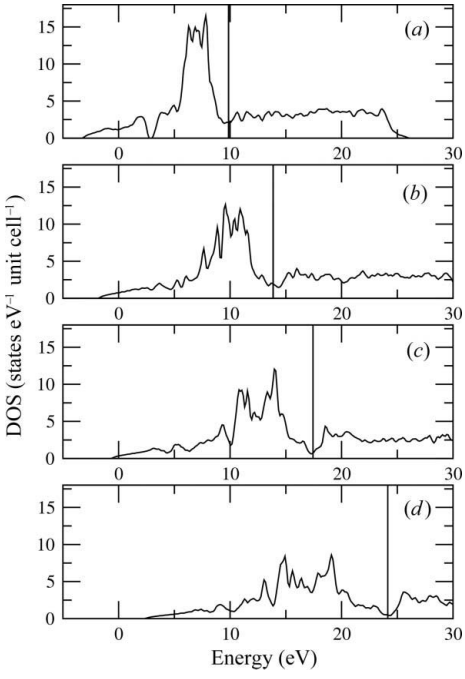

Figure 7
Total electronic density of states for phases derived from simulations starting with the orthorhombic *Pnma*-I MnP structure: (*a*) *Pnma*-I (MnP) phase at 12 Å^3 atom^{-1} (~4 GPa), (*b*) phase *Pnma*-II (FeB) at 9.5 Å^3 atom^{-1} (~62 GPa), (*c*) phase *Pnma*-III (FeB) at 8 Å^3 atom^{-1} (~147 GPa) and (*d*) phase *Pnma*-III (FeB) at 6 Å^3 atom^{-1} (~503 GPa). The vertical lines show the positions of the Fermi energy.

3.4. Crystal structures of the high-pressure phases of NiSi with *Pbma* and *P*4/*nmm* symmetry, derived from decompression of a structural variant of *Pnma*-III (FeB): phases *Pbma*-I and *P*4/*nmm* (CuTi)

The realization that the high-pressure phases of NiSi discussed in §3.3 could be described as originating from hexagonal close packing led us to carry out simulations for the crystal structure shown in Fig. 8(*a*). The space group of this new arrangement, which was produced by exchanging the coordinates of half of the Ni and Si atoms in the *Pnma*-III unit cell, is *Pbma* (or *Pbcm* in the conventional setting). This structure is similar to the *Pnma*-III structure shown in Fig. 6(*d*) in that, at the highest pressures, all atoms still ideally have 12 nearest neighbours in anticuboctahedral coordination. However, in the *Pnma*-III structure, eight of these neighbours are atoms of a different kind and four are atoms of the same

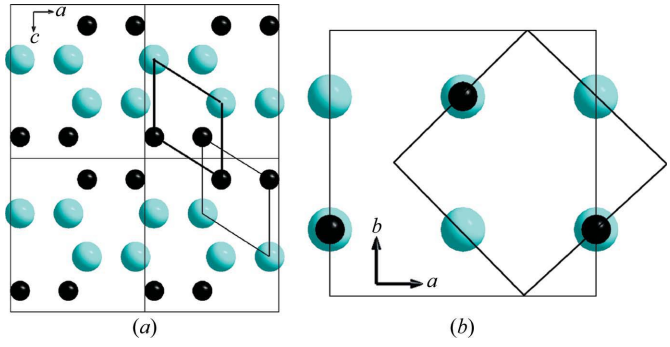

Figure 8
(*a*) The high-pressure *Pbma*-I structure of NiSi at 5.25 Å^3 atom^{-1} (~812 GPa), showing its relationship to that of *Pnma*-III (FeB) (Fig. 6*d*). This structure is also formed by stacking of pseudo-close-packed layers as shown in Fig. 6(*c*), but in this case the arrangement is such that the primary 12-fold coordination of each atom involves equal numbers of Ni and Si atoms. As before, heavy and light lines outline the pseudo-cells of the layers at $y = \frac{1}{4}$ and $y = \frac{3}{4}$, respectively, and the Si atoms are depicted by the smaller darker spheres. Note that, so as to conform to the conventional choice of origin in the two space groups, with the centre of symmetry at the origin of the unit cell, the *z* coordinates of the atoms in the two structures are related by $z(Pbma) = z(Pnma) - 0.25$. (*b*) The low-pressure *P*4/*nmm* (CuTi) structure of NiSi at 11.75 Å^3 atom^{-1} (~0.6 GPa), viewed along [001]. Both the orthorhombic (*Pbma*) simulation cell and the tetragonal (*P*4/*nmm*) unit cell (origin at $\bar{4}m2$) are outlined. As before, the Si atoms are depicted by the smaller darker spheres.

kind, whereas in the *Pbma*-structured phase, the 12 nearest neighbours consist of equal numbers of Ni and Si atoms. An alternative method for generating this structure would be to imagine that the alternative location was used for successive close-packed layers in the stack, *i.e.* the layers would have an *ACACAC* sequence (rather than the *ABABA* sequence in *Pnma*-III). Inspection of the Inorganic Crystal Structure Database (ICSD; Fletcher *et al.*, 1996) did not reveal any binary compounds with space group *Pbma* and atoms arranged as shown in Fig. 8(*a*) and we therefore refer to this structure as phase *Pbma*-I.

Simulation of this structure at the highest pressure considered (V = 5.25 Å^3 atom^{-1}, ∼812 GPa) showed the expected 12-fold coordination of all atoms, at distances ranging from 1.88 to 2.04 Å. Further simulations at increasing volumes revealed a phase transition, which appears to be continuous in nature, at ∼61 GPa (∼10.5 Å^3 atom^{-1}) as shown by the cell parameters plotted in Fig. 2(*b*). The fractional coordinates from these simulations are shown in Fig. 9. Inspection of the structure at the largest volume considered (12.5 Å^3 atom^{-1}), both visually and using the program *Endeavour* (Putz *et al.*, 1999; Crystal Impact, 2010), showed that the space group of the low-pressure phase was *P*4/*nmm* (a supergroup of *Pbma*), with Z = 2 and cell parameters related to those of the orthorhombic phase by $a_O = b_O = 2^{1/2}a_T$ and $c_O = c_T$ (where the subscripts O and T refer to the orthorhombic and tetragonal structures, respectively). Comparison with the ICDD database (Fletcher *et al.*, 1996) revealed that the structure [shown in Fig. 8(*b*) for a volume of 11.75 Å^3 atom^{-1}, ∼0.6 GPa] was of the CuTi type (see *e.g.* Karlsson, 1951), although the local coordination of the atoms may differ somewhat from that found in CuTi itself; we therefore refer to this phase as *P*4/*nmm* (CuTi). In this structure, Ni is sixfold coordinated by Si atoms and Si is sixfold coordinated by Ni atoms [in both cases at distances between 2.35 and 2.40 Å for the structure shown in Fig. 8(*b*)], but both coordination polyhedra are now distorted octahedra.

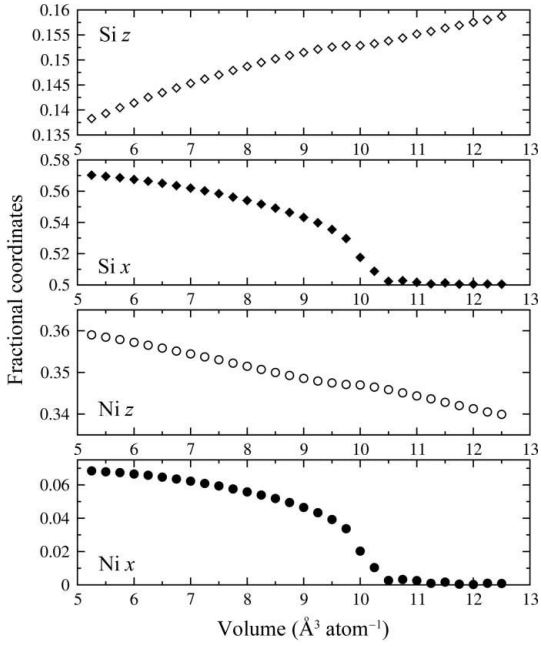

Figure 9
Fractional atomic coordinates of NiSi as a function of volume for simulations starting with the orthorhombic *Pbma*-I structure; the transition to the tetragonal low-pressure phase (*P*4/*nmm*, CuTi) is clearly visible [the corresponding cell parameters are shown in Fig. 2(*b*)].

3.5. Crystal structures of the high-pressure phases of NiSi, derived from compression of the 'anti-MnP' structure: phases *Pnma*-IV and *Pnma*-III (FeB)

In this set of simulations, the starting structure was that of the ambient-pressure *Pnma*-I (MnP) phase of NiSi, but with the fractional coordinates of all of the Ni and Si atoms exchanged. As might be expected from inspection of Figs. 6(*c*) and 6(*d*) (in which interchange of the atomic symbols can be seen to produce an essentially identical structure), this structure spontaneously transformed into the isosymmetric *Pnma*-III (FeB) form of NiSi as the unit-cell volume was reduced (with an origin shift of *c*/2). The transformation, however, occurred at a much larger volume and lower pressure, V < 11.5 Å^3 atom^{-1} (∼5 GPa), than was the case for simulations in which the experimentally observed *Pnma*-I (MnP) phase of MnP was compressed. The evolution of the lattice parameters and fractional coordinates can be seen in Figs. 2(*a*) and 10, respectively.

The low-pressure structure from these simulations, existing in the volume range 11.5 < V < 15 Å^3 atom^{-1}, is here termed phase *Pnma*-IV. As can be seen from Fig. 1 and Table 1, this is

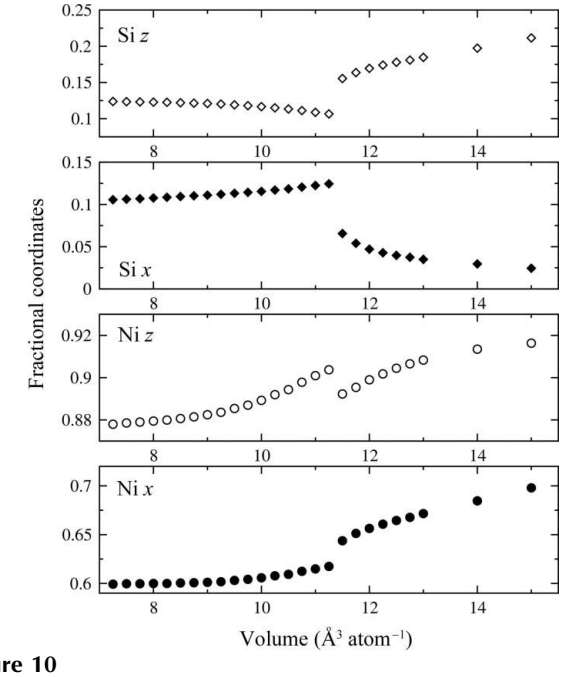

Figure 10
Fractional atomic coordinates of NiSi as a function of volume for simulations starting with an orthorhombic *Pnma* 'anti-MnP' structure; the transition from the low-pressure phase (*Pnma*-IV) to the high-pressure *Pnma*-III (FeB) structure is clearly visible [the corresponding cell parameters are shown in Fig. 2(*a*)]. Note that the coordinates of Ni and Si in the high-pressure *Pnma*-III (FeB) structure are interchanged with respect to those shown in Fig. 5.

one of the least thermodynamically stable phases of NiSi simulated and, therefore, its crystal structure has not been considered in any detail. The main difference between this *Pnma*-IV structure (at 12.15 Å^3 atom^{-1}) and that of the MnP structure seems to be that the primary coordination number of the Si atoms is increased from six in the *Pnma*-I (MnP) phase to eight in the *Pnma*-IV phase by the approach of two Si atoms which were previously next nearest neighbours.

3.6. Other structures derived from close packing: the WC, NiAs and anti-NiAs structures

The realization that the hypothetical high-pressure phases of NiSi, *Pnma*-III (FeB) and *Pbma*-I, could be considered as being based on hexagonal close packing led us to also carry out simulations for a crystal structure composed of *ABAB* stacking of layers, each of which was composed of atoms of only one type. This arrangement corresponds to that found in hexagonal WC and has space group $P\overline{6}m2$ (Leciejewicz, 1961). It was found that this phase was never thermodynamically stable and it is not discussed further here. Similarly, simulations of NiSi in the hexagonal NiAs and anti-NiAs structures (space group $P6_3/mmc$) showed that neither of these phases was ever thermodynamically stable.

3.7. Crystal structure of the cubic ε-FeSi and CsCl phases of NiSi

Fig. 3 shows that, between about 50 and 150 GPa, the ε-FeSi structure is almost the thermodynamically stable structure of NiSi. It is interesting to note that in very early work (Borén, 1933) it was reported that NiSi crystallized with this structure at atmospheric pressure, a result that does not, however, appear ever to have been reproduced. The ε-FeSi structure is cubic with space group $P2_13$ and is unusual in that each atom is sevenfold coordinated by atoms of the other kind. In its idealized form this sevenfold coordination is perfect, with the coordinating atoms lying at seven of the 20 vertices of pentagonal dodecahedra. In the ε-FeSi crystal structure both atoms occupy 4*a* (x, x, x) sites. The value of x required to produce ideal sevenfold coordination is given by $x = \pm 1/4\tau$, where τ is the golden ratio, $(1 + 5^{1/2})/2$ [see *e.g.* Vočadlo *et al.* (1999) for a fuller description of the ε-FeSi structure]. Fig. 11 shows the changes in fractional coordinates as a function of pressure for simulations of both ε-FeSi itself (results from Vočadlo *et al.*, 1999) and the ε-FeSi structure of NiSi (present work). It can be seen that neither structure tends exactly to the coordinates required for ideal sevenfold coordination but that, throughout the whole of the pressure range considered, the NiSi phase more closely approaches the ideal form. For comparison with previous calculations (Vočadlo *et al.*, 1999), the total electronic density of states for NiSi in the ε-FeSi structure at ∼96 GPa (8.75 Å^3 atom^{-1}) is shown in Fig. 12, together with that for the CsCl structure (at ∼267 GPa, 7.0 Å^3 atom^{-1}). It can be seen that both of these phases are metallic although, as for the *Pnma* phases I–III (Fig. 7), the Fermi energies lie close to minima in the DOS.

At pressures above ∼247 GPa (Fig. 3), our simulations show that the stable phase of NiSi is that with the CsCl structure. This is an important result as it implies that, at pressures equivalent to those in the Earth's inner core ($329 \leq P \leq 364$ GPa), NiSi and FeSi will be isostructural. However, the pressure required to stabilize the CsCl structure in NiSi is much greater than that required in FeSi. In FeSi, similar athermal *ab initio* simulations gave a transition pressure between the ε-FeSi and CsCl phases of between 13 GPa (Vočadlo *et al.*, 1999) and 30–40 GPa (Caracas & Wentzcovitch, 2004), whilst experiments showed that nearly pure CsCl-structured FeSi could be synthesized in a multi-anvil press at 24 GPa and 2023 K (Dobson *et al.*, 2002; see also Lord *et al.*, 2010). In the present case, the pressure required to form the

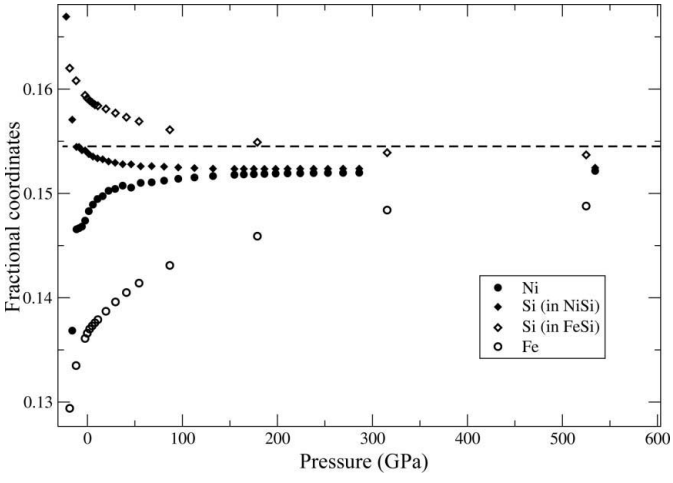

Figure 11
Fractional atomic coordinates of NiSi and FeSi (Vočadlo *et al.*, 1999) in the cubic $P2_13$ ε-FeSi structure (note that for convenience the modulus of the coordinates is plotted). The value required for an ideal sevenfold-coordinate structure is shown by the horizontal line; for further details see Vočadlo *et al.* (1999).

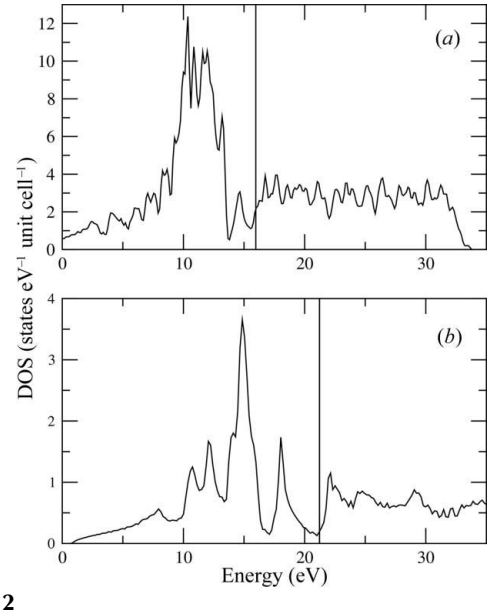

Figure 12
Total electronic density of states for NiSi in (*a*) the ε-FeSi structure at 8.75 Å^3 atom^{-1} (∼96 GPa) and (*b*) the CsCl structure at 7.0 Å^3 atom^{-1} (∼267 GPa). The vertical lines show the positions of the Fermi energy.

CsCl-structured phase of NiSi estimated from the *ab initio* simulations (∼247 GPa) appears to be rather greater than that required to synthesize the material in laser-heated diamond-anvil-cell experiments (∼60 GPa; Lord *et al.*, 2012), indicating that the Clapeyron slope of the phase boundary is negative.

3.8. The high-P phase diagram of NiSi: chemical and physical properties and geophysical consequences

Before discussing the predicted behaviour of NiSi at high pressure, it is useful to consider how well our simulations predict the properties of this material at atmospheric pressure. Figs. 1 and 3 show that the stable phase under these conditions has the MnP structure (phase *Pnma*-I), as found experimentally, and Table 2 shows that our relaxed atomic fractional coordinates are in good agreement with those determined by X-ray crystallography (see §3.2). The value of the incompressibility obtained in the present work (161 GPa) is in good agreement with that found in previous simulations (168–175 GPa; Connétable & Thomas, 2009), bearing in mind the differences in simulation methodology and equations of state used, and also with the experimental value of 153 (14) GPa obtained very recently in a preliminary investigation of NiSi at high pressure using a diamond anvil cell (Lord *et al.*, 2012). In common with the known electrical properties of NiSi and the results of previous simulations, we find that NiSi is metallic and our density of states (Fig. 7*a*) is in qualitative agreement with that of Connétable & Thomas (2009). We believe, therefore, that our simulations have produced an accurate representation of the structure and properties of the material in its ambient-pressure phase, and that the other structures have been simulated equally well.

At very high pressures, Fig. 3 shows that NiSi will adopt the CsCl structure. This result would also appear to be robust, as the form of the relative enthalpy curves is such that the stability of the CsCl phase is increasing as pressure increases. Thus, although the exact value of the transition pressure may vary according to the details of the simulation methodology, it seems highly likely that such a transition must occur. In this respect the expected behaviour of NiSi is identical to that of FeSi. However, previous *ab initio* simulations of FeSi (Vočadlo *et al.*, 1999) showed that the CsCl phase became stable, relative to the ε-FeSi structure, at a very much lower pressure (13 GPa). In NiSi, the CsCl structure is not predicted to become stable relative to the ε-FeSi structure until above 170 GPa. While it seems highly probable, therefore, that an (Fe,Ni)Si solid solution with the CsCl structure will exist at high pressures, it is possible that the addition of relatively small amounts of Ni to FeSi may significantly affect its phase diagram.

In the region between ∼20 and ∼250 GPa, we can be less certain about the form of the phase diagram of NiSi. The reason for this is twofold; firstly, the enthalpy differences between, for example, the ε-FeSi-structured phase and that which we refer to as *Pbma*-I are small, being as little as 8 meV atom^{-1}. Secondly, our calculations are athermal and so can take no account of the Clapeyron slopes of the phase boundaries; since these are likely to differ for the different phases it is quite possible that a different sequence of structures might be found by experiment [in this connection, we note that in the laser-heated diamond-anvil-cell study of NiSi by Lord *et al.* (2012) it was found that the ε-FeSi-structured phase of NiSi formed above ∼18 GPa at ∼1700 K and that the CsCl-structured phase formed above ∼60 GPa and ∼2500 K; however, very recent investigations of NiSi at high P and T using a multi-anvil press by J. Ahmed (personal communication) have indicated that, while the ε-FeSi-structured phase is stable at ∼18 GPa and ∼1770 K, a tetragonal phase, as yet not fully characterized but probably related to the *P*4/*nmm* structure found in the present work, may form at ∼18 GPa and ∼1300 K]. In comparison with FeSi, the present *ab initio* study suggests that a wider range of coordination numbers may be found in NiSi as pressure increases. Structures in which all atoms are sixfold (*Pnma*-I, MnP; *P*4/*nmm*, CuTi), 12-fold (*Pbma*-I and *Pnma*-III, FeB) and eightfold (CsCl) coordinated are predicted to be thermodynamically stable, and the ε-FeSi-structured phase, in which all atoms are sevenfold coordinated, has only a slightly higher enthalpy.

The importance of the present study for the role of nickel and silicon in the deep Earth depends to a large extent on the question of whether or not FeSi itself plays a significant role. As discussed by, for example, Lord *et al.* (2010) it has been suggested that FeSi might occur in the D″ layer, just above the core–mantle boundary, and that within this region of the Earth both solid and liquid FeSi will probably be present. Throughout the underlying outer core, FeSi will be in the liquid state. The pressure range from the top of D″ to the bottom of the outer core extends from about 118 to 329 GPa and thus spans the region where NiSi solid phases with several different coordination numbers may exist. It would be of interest to determine to what extent similar changes in coordination number might occur in the liquid phase of NiSi at these pressures; radial distribution functions have been measured for liquid NiSi by neutron diffraction, but only at ambient pressure (Gruner *et al.*, 2009). However, when considering the structure that would be adopted by NiSi under the conditions of the Earth's core it is, of course, essential to also consider the effect of temperature on the phase diagram. The recent experimental study of Lord *et al.* (2012) indicates that the Clapeyron slopes of the phase boundaries between the CsCl-structured phase of NiSi and its lower-pressure polymorphs must be negative, as is the case for FeSi (Dobson *et al.*, 2002; Santamaría-Pérez & Boehler, 2008; Lord *et al.*, 2010). If this supposition is correct, it is quite possible that CsCl-structured NiSi would be the stable phase throughout the whole of the core region.

Within the inner core, CsCl-structured FeSi is expected to be solid, but there is some debate as to whether or not it might be present in appreciable amounts – see Lord *et al.* (2010) for discussion of this point. The pressure in the inner core ranges between about 329 and 364 GPa. Using the equation of state parameters for CsCl-structured FeSi (Vočadlo *et al.*, 1999) and those for the CsCl-structured phase of NiSi listed in Table 1, we find (assuming the thermal expansion of both materials to

be identical at inner-core pressures) that NiSi will be 6% denser than FeSi throughout the inner core, with roughly half of this density difference arising from the greater mass of the Ni atom. However, this conclusion should be treated with some caution, requiring further simulations and experiments to determine the *PVT* equation of state of this high-pressure polymorph of NiSi in order to fully quantify any differences between its physical properties and those of the equivalent phase of FeSi.

References

Acker, J., van den Berg, G. J. K., Bohmhammel, K., Kloc, Ch. & van Miltenburg, J. C. (1999). *Thermochim. Acta*, **339**, 29–33.

Bhattacharya, B. & Masson, D. B. (1976). *Mater. Sci. Eng.* **22**, 133–140.

Birch, F. (1964). *J. Geophys. Res.* **69**, 4377–4388.

Bjurstroem, T. & Arnfelt, H. (1929). *Z. Phys. Chem. B*, **4**, 469–476.

Blöchl, P. E. (1994). *Phys. Rev. B*, **50**, 17953–17979.

Borén, B. (1933). *Ark. Kem. Mineral. Geol. A*, **11**, 1–28.

Caracas, R. & Wentzcovitch, R. (2004). *Geophys. Res. Lett.* **31**, L20603.

Connétable, D. & Thomas, O. (2009). *Phys. Rev. B*, **79**, 094101.

Connétable, D. & Thomas, O. (2010). *Phys. Rev. B*, **81**, 075213.

Connétable, D. & Thomas, O. (2011). *J. Alloys Compd.* **509**, 2639–2644.

Crystal Impact (2010). *Endeavour*. Version 1.3e. Crystal Impact GbR, Bonn, Germany, http://crystalimpact.com/endeavour.

De Keyser, K., Van Bockstael, C., Detavernier, C., Van Meirhaeghe, R. L., Jordan-Sweet, J. & Lavoie, C. (2008). *Electrochem. Solid State Lett.* **11**, H266–H268.

Detavernier, C., Lavoie, C. & d'Heurle, F. M. (2003). *J. Appl. Phys.* **93**, 2510–2515.

Dobson, D. P., Crichton, W. A., Bouvier, P., Vočadlo, L. & Wood, I. G. (2003). *Geophys. Res. Lett.* **30**, 1014.

Dobson, D. P., Vočadlo, L. & Wood, I. G. (2002). *Am. Mineral.* **87**, 784–787.

Errandonea, D., Santamaría-Perez, D., Vegas, A., Nuss, J., Jansen, M., Rodríguez-Hernandez, P. & Muñoz, A. (2008). *Phys. Rev. B*, **77**, 094113.

Fletcher, D. A., McMeeking, R. F. & Parkin, D. (1996). *J. Chem. Inf. Comput. Sci.* **36**, 746–749.

Gruner, S., Marczinke, J., Hennet, L., Hoyer, W. & Cuello, G. J. (2009). *J. Phys. Condens. Matter*, **21**, 385403.

d'Heurle, F., Petersson, C. S., Baglin, J. E. E., La Placa, S. J. & Wong, C. Y. (1984). *J. Appl. Phys.* **55**, 4208–4218.

Hohenberg, P. & Kohn, W. (1964). *Phys. Rev.* **136**, B864–B871.

Karlsson, N. (1951). *J. Inst. Met.* **79**, 391–405.

Kresse, G. & Furthmüller, J. (1996). *Phys. Rev. B*, **54**, 11169–11186.

Kresse, G. & Joubert, D. (1999). *Phys. Rev. B*, **59**, 1758–1775.

Lavoie, C., Detavernier, C., Cabral, C., d'Heurle, F. M., Kellock, A. J., Jordan-Sweet, J. & Harper, J. M. E. (2006). *Microelectron. Eng.* **83**, 2042–2054.

Leciejewicz, J. (1961). *Acta Cryst.* **14**, 200.

Li, B., Luo, Z., Shi, L., Zhou, J., Rabenburg, L., Ho, P. S., Allen, R. A. & Cresswell, M. W. (2009). *Nanotechnology*, **20**, 085304.

Lord, O. T., Vočadlo, L., Wood, I. G., Dobson, D. P., Clark, S. M. & Walter, M. J. (2012). *J. Appl. Cryst.* **45**. Submitted.

Lord, O. T., Walter, M. J., Dobson, D. P., Armstrong, L., Clark, S. M. & Kleppe, A. (2010). *J. Geophys. Res.* **115**, B06208.

McDonough, W. F. & Sun, S. (1995). *Chem. Geol.* **120**, 223–253.

Murray, C. E., Zhang, Z. & Lavoie, C. (2009). *J. Appl. Phys.* **106**, 073521.

Perrin, C., Mangelinck, D., Nemouchi, F., Labar, J., Lavoie, C., Bergman, C. & Gas, P. (2008). *Mater. Sci. Eng. B*, **154–155**, 163–167.

Perrin, C., Nemouchi, F., Clugnet, G. & Mangelinck, D. (2007). *J. Appl. Phys.* **101**, 073512.

Pippard, A. B. (1966). *The Elements of Classical Thermodynamics*, pp. 43–45. Cambridge University Press.

Poirier, J.-P. (1994). *Phys. Earth Planet. Inter.* **85**, 319–337.

Putz, H., Schön, J. C. & Jansen, M. (1999). *J. Appl. Cryst.* **32**, 864–870.

Rabadanov, M. Kh. & Ataev, M. B. (2002*a*). *Crystallogr. Rep.* **47**, 40–45.

Rabadanov, M. Kh. & Ataev, M. B. (2002*b*). *Crystallogr. Rep.* **47**, 424–427.

Rundqvist, S. (1962). *Acta Chem. Scand.* **16**, 287–292.

Saltykov, V., Nuss, J., Konuma, M. & Jansen, M. (2009). *Z. Anorg. Allg. Chem.* **635**, 70–75.

Santamaría-Pérez, D. & Boehler, R. (2008). *Earth Planet. Sci. Lett.* **265**, 743–747.

Teyssier, J., Viennois, R., Salamin, J., Giannini, E. & van der Marel, D. (2008). *J. Alloys Compd.* **465**, 462–467.

Toman, K. (1951). *Acta Cryst.* **4**, 462–464.

Van Bockstael, C., De Keyser, K., Van Meirhaeghe, R. L., Detavernier, C., Jordan-Sweet, J. & Lavoie, C. (2009). *Appl. Phys. Lett.* **94**, 033504.

Vočadlo, L., Brodholt, J. P., Dobson, D. P., Knight, K. S., Marshall, W. G., Price, G. D. & Wood, I. G. (2002). *Earth Planet. Sci. Lett.* **203**, 567–575.

Vočadlo, L., Knight, K. S., Price, G. D. & Wood, I. G. (2002). *Phys. Chem. Miner.* **29**, 132–139.

Vočadlo, L., Price, G. D. & Wood, I. G. (1999). *Acta Cryst.* B**55**, 484–493.

Wang, Y. & Perdew, J. (1991). *Phys. Rev. B*, **44**, 13298–13307.

Wells, A. F. (1986). *Structural Inorganic Chemistry*, 5th ed., pp. 158–161. Oxford: Clarendon Press.

Wilson, D. F. & Cavin, O. B. (1992). *Scr. Metall. Mater.* **26**, 85–88.

Wood, I. G., Vočadlo, L., Knight, K. S., Dobson, D. P., Marshall, W. G., Price, G. D. & Brodholt, J. (2004). *J. Appl. Cryst.* **37**, 82–90.

Wu, H., Kratzer, P. & Scheffler, M. (2005). *Phys. Rev. B*, **72**, 14425.